# Microseismicity, stress, and fracture in the Coso geothermal field, California

Qiuchun Feng *, Jonathan M. Lees

*Department of Geology and Geophysics, Yale University, New Haven, CT 06511, USA*

## Abstract

Microseismicity, stress, and fracture in the Coso geothermal field are investigated using seismicity, focal mechanisms and stress analysis. Comparison of hypocenters of microearthquakes with locations of development wells indicates that microseismic activity has increased since the commencement of fluid injection and circulation. Microearthquakes in the geothermal field are proposed as indicators of shear fracturing associated with fluid injection and circulation along major pre-existing fractures. High-seismicity zones are associated with the main fluid-flow paths within the geothermal system. Calculated stress patterns from focal mechanisms provide direct evidence for the boundary between significantly different stress regimes within the Coso geothermal field. Microseismicity in the Coso geothermal field is spatially but not temporally related to regional seismicity extending southeast of the field. The spatial distribution of these events defines a northwest-trending seismic-fracture zone, consistent with a previously defined northwest-striking zone. The abrupt decrease of seismicity below this fracture zone may provide seismic evidence for the existence of a brittle and ductile transition zone at shallow depth beneath the Coso geothermal field. © 1998 Elsevier Science B.V. All rights reserved.

*Keywords:* induced seismicity; geothermal; stress distribution; microearthquakes

## 1. Introduction

The Coso area is located in eastern California on the western edge of the Basin and Range (Fig. 1). The geothermal field is confined to a nearly north–south-trending zone between Sugarloaf Mountain and Coso Hot Springs (Duffield et al., 1980; Bishop and Bird, 1987). Recent geothermal energy development has resulted in more than 90 operating wells (Wohletz and Heiken, 1992). The production of geothermal energy is dynamic and involves injecting fluid underground and extracting hot fluid from neighboring production wells. Transport of injected

\* Corresponding author.

fluid through pre-existing fractures may substantially change local stress regimes, cause shearing, and induce microseismicity (Pearson, 1981; Cornet and Julien, 1989; Fehler, 1989; Jupe et al., 1992).

A joint effort of seismological monitoring at the geothermal field, using a 16-station Digital Seismic Network, is being conducted by the Geothermal Program Office of the Naval Air Weapon Station and the California Energy Company, Inc. From 1991 to 1995, more than 20,000 microearthquakes were recorded by the Digital Seismic Network. The intensive microseismic activity indicates an active fracturing process that can be associated with the injection and circulation of fluids within the geothermal system. Locations of fracture zones and knowledge of
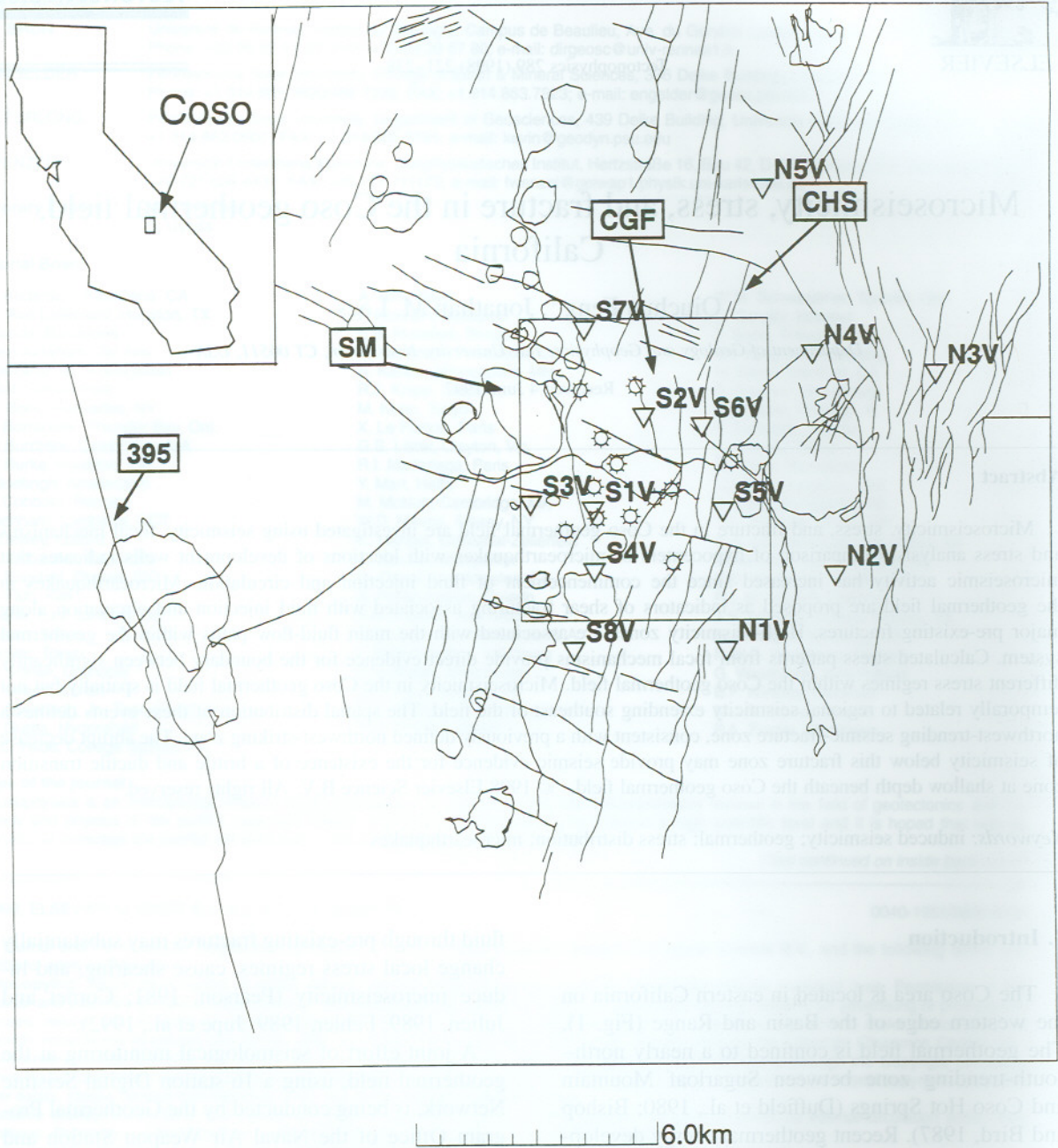
Fig. 1. Generalized map of the Coso geothermal field and the vicinity, including major faults (short lines) and late Cenozoic domes (closed lines), the seismic stations (triangles) of the Coso Digital Seismic Network, and development wells (circles). The box outlines the principal geothermal area. *CGF* = Coso geothermal field; *CHS* = Coso Hot Springs; *SM* = Sugarloaf Mountain.

the predominant orientation of fractures are vital for understanding fluid flow and heat exchange within the geothermal system.

Induced microseismicity is primarily associated with shear failure along pre-existing fractures due to pressurized pore fluids (Pearson, 1981; Fehler,

1989) that are oriented with respect to ambient stress (Fehler, 1989; Jupe et al., 1992). It is possible to determine the local state of stress and orientation of pre-existing fractures which can subsequently be used to determine main fluid-flow paths within the geothermal system (Fehler, 1989). In this paper we use seismic data to estimate the present state of stress in the Coso geothermal field and its vicinity, and to infer orientations of major fracture zones associated with geothermal fluid transport.

## 2. Geologic setting and regional seismicity

The Coso geothermal field is characterized by the presence of a variety of late Cenozoic volcanic rocks. Recent lava flows and rhyolite domes overlie a basement complex of late Mesozoic plutons and metamorphic rocks extensively exposed in this area (Duffield et al., 1980). The geothermal field contains three major sets of faults believed to be control structures for subsurface hydrothermal fluid circulation (Roquemore, 1984; Bishop and Bird, 1987). The first set consists of dextral strike-slip motion trending west-northwest and is well developed to the south and northwest of the geothermal field (Fig. 1) (Duffield et al., 1980; Roquemore, 1984). The second set includes normal faults striking north to northeast and is well developed throughout the geothermal field (Fig. 1). The third set comprises northeast sinistral strike-slip motion trending northeast from the geothermal field (see Roquemore, 1984).

The Coso region is one of the most active seismic areas in southern California with a regional stress state of north–south compression and east–west extension (Walter and Weaver, 1980). Using 4216 seismic events with magnitude from 0.5 to 3.9 (1975–1977), Walter and Weaver (1980) showed that active seismic zones strike radially outward from the Pleistocene rhyolite field, and most earthquakes locate at depths of 1 to 8 km in a zone with approximate northwest orientation. Within the geothermal area, fault-plane solutions exhibited mainly normal faulting trending north-northeast with a small component of strike slip (Walter and Weaver, 1980). From 1981 to 1994, more than 5000 earthquakes with magnitudes from 0 to 4 have been recorded by the Southern California Seismic Network (SCSN), operated by CalTech and the U.S.G.S., indicating

continuous, active east–west extension in this region.

Geochemical analyses of production fluids and fluid inclusions show that flow emanates from the deeper sections in the southern part of the field and shoals towards the north (Moore et al., 1989). Surface exposures of vents and fumaroles are evident at Coso Hot Springs (Fig. 1) northeast of the main producing field. In the southern production wells, temperatures exceeding 300°C are common at 1.5–2 km depth, whereas the northern wells produce from shallower depths (0.5–1.0 km) and at lower temperatures (<250°C). Steep gradients of Cl concentrations and $CO_2$ also delineate southern versus northern production in the field.

## 3. Seismic data and data processing

Two seismic data sets, Coso Geothermal Data (CGD) and CalTech Data (CITD), were analyzed in this study. The CGD was obtained by the Coso Digital Seismic Network from July 1991 to January 1995 and includes more than 20,000 microearthquakes concentrated in the geothermal field. CITD was obtained by SCSN (Southern California Seismic Network) from December 1981 to March 1994 and includes more than 5000 local and regional events distributed in the Coso vicinity. All events were relocated with a one-dimensional, layered, Coso regional velocity model (Table 1) and all events with less than

Table 1
Coso regional velocity model

| P-depth (km) | P-velocity (km/s) | S-velocity (km/s) |
|---|---|---|
| 0.0 | 1.82 | 1.05 |
| 0.09 | 2.76 | 1.59 |
| 0.15 | 3.67 | 2.12 |
| 0.31 | 4.34 | 2.50 |
| 0.52 | 5.0 | 2.90 |
| 1.22 | 5.32 | 3.07 |
| 2.44 | 5.58 | 3.22 |
| 3.66 | 5.77 | 3.33 |
| 5.48 | 5.99 | 3.46 |
| 12.19 | 6.05 | 3.49 |
| 15.00 | 7.20 | 4.15 |
| 18.28 | 8.00 | 4.62 |

The 1-D velocity model is derived by simple travel-time inversion using constraints from well-log data and vertical seismic profiles (P. Malin, Duke University, pers. commun., 1994).
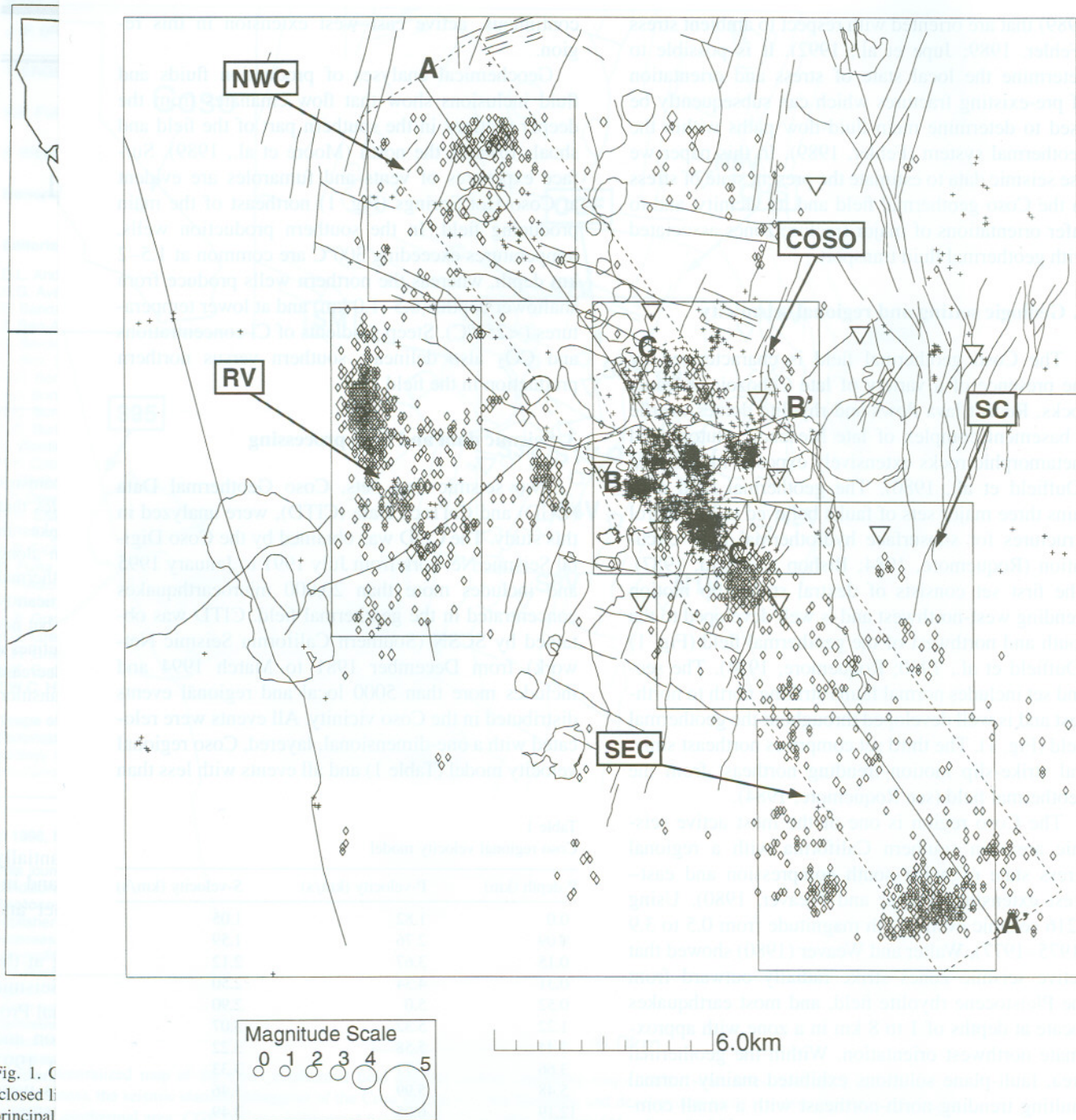
Fig. 1. C
(closed li
principal

Fig. 2. (a) Spatial distribution of seismicity from the Coso Digital Seismic Network (plus signs) and SCSN (diamond signs) used in this study. NWC, RV, SC, and SEC denote the 4 seismic zones, and COSO denotes the Coso geothermal field. The dashed box with line indicates the position of the A–A′ vertical section. (b). Detailed map of the principal geothermal area outlined by COSO with index of the six seismic zones, COSO-N, COSO-C, COSO-NE, COSO-NW, COSO-SW, and COSO-SE. B–B′ and C–C′ denote the positions of the vertical sections.
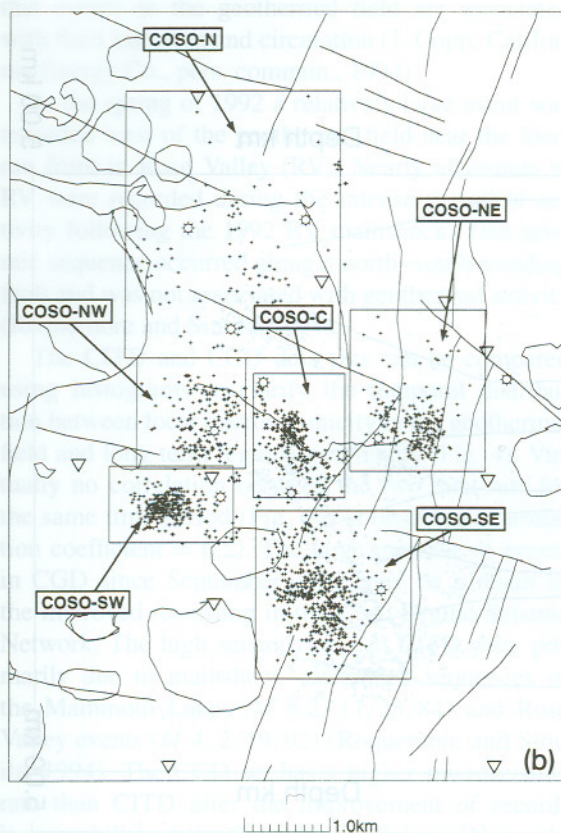
the pre
underst
the geo

Fig. 2 (continued).

eight first P-wave arrivals were excluded. For this study, 2967 high-quality events were selected from CGD and CITD for comparison of seismicity, focal mechanism analysis, and stress analysis (Fig. 2a).

To facilitate comparison of spatial variations of microseismicity, focal mechanisms, and stress orientations, we divided the Coso area into ten zones according to spatial concentrations (cluster patterns) of seismic activity (Fig. 2). Zones labeled NWC, RV, SC, and SEC are regional clusters where as COSO-N, COSO-C, COSO-NE, COSO-NW, COSO-SE, and COSO-SW are clusters within the geothermal field (Fig. 2b). Events within a single zone are presumably influenced by similar stress regimes and should possess correspondingly similar focal mechanisms (Cornet and Julien, 1989; Castillo and Zoback, 1995). A standard grid-search program called FPFIT (Reasenberg and Oppenheimer, 1985) was used to calculate focal mechanisms for these se-

lected events. Stress inversion (Michael, 1984) was applied to each focal mechanism subset to determine local stress in each zone. The inversion scheme determines the orientation of three principal stress axes and the stress ratio ($\phi$) by minimizing the misfit angle ($\beta$) between the direction of the predicted shear stress on the fault plane and the observed slip direction on each plane determined from focal mechanisms. The stress ratio measures the relative magnitude of three principal stresses, $S1$ (most compressive), $S2$, and $S3$ (most extensive), using this equation:

$$\phi = \frac{S2 - S3}{S1 - S3}$$

The stress ratio varies from 0 to 1, where a ratio of 0 represents compression compensated by isotropic extension in the plane normal to $S1$ and a ratio of 1 indicates extension compensated by isotropic compression in the plane normal to $S3$ (Seeber and Armbruster, 1995). The 95% confidence limits for the orientations of the principal stresses were calculated using a bootstrap resampling technique (Michael, 1987a,b) by assuming that 10% of the selected slip planes were picked incorrectly.

## 4. Induced microseismicity

Hypocenter locations of selected events in the Coso geothermal field and vicinity are shown in Fig. 2. Except for events in Rose Valley (RV), most earthquakes in the Coso region are located within a zone that strikes approximately northwest through the geothermal field along cross-section A–A′ (Fig. 2a). Focal depths of these events increase with distance from the geothermal field and extend northwest and southeast, forming a continuous seismic zone (vertical section A–A′ in Fig. 3), consistent with the northwest-striking seismic zone defined by Walter and Weaver (1980). Hypocenters within the geothermal field are shallower and denser than those in the outlying regions (Fig. 2a, Fig. 3). Tight clusters of seismic events are prevalent near geothermal boreholes (Fig. 2b, and vertical sections B–B′ and C–C′ in Fig. 3), consistent with mapped zones of high fluid-flow entries in production wells (Bishop and Bird, 1987). The spatial and temporal distribution of microseismicity in the Coso region suggests
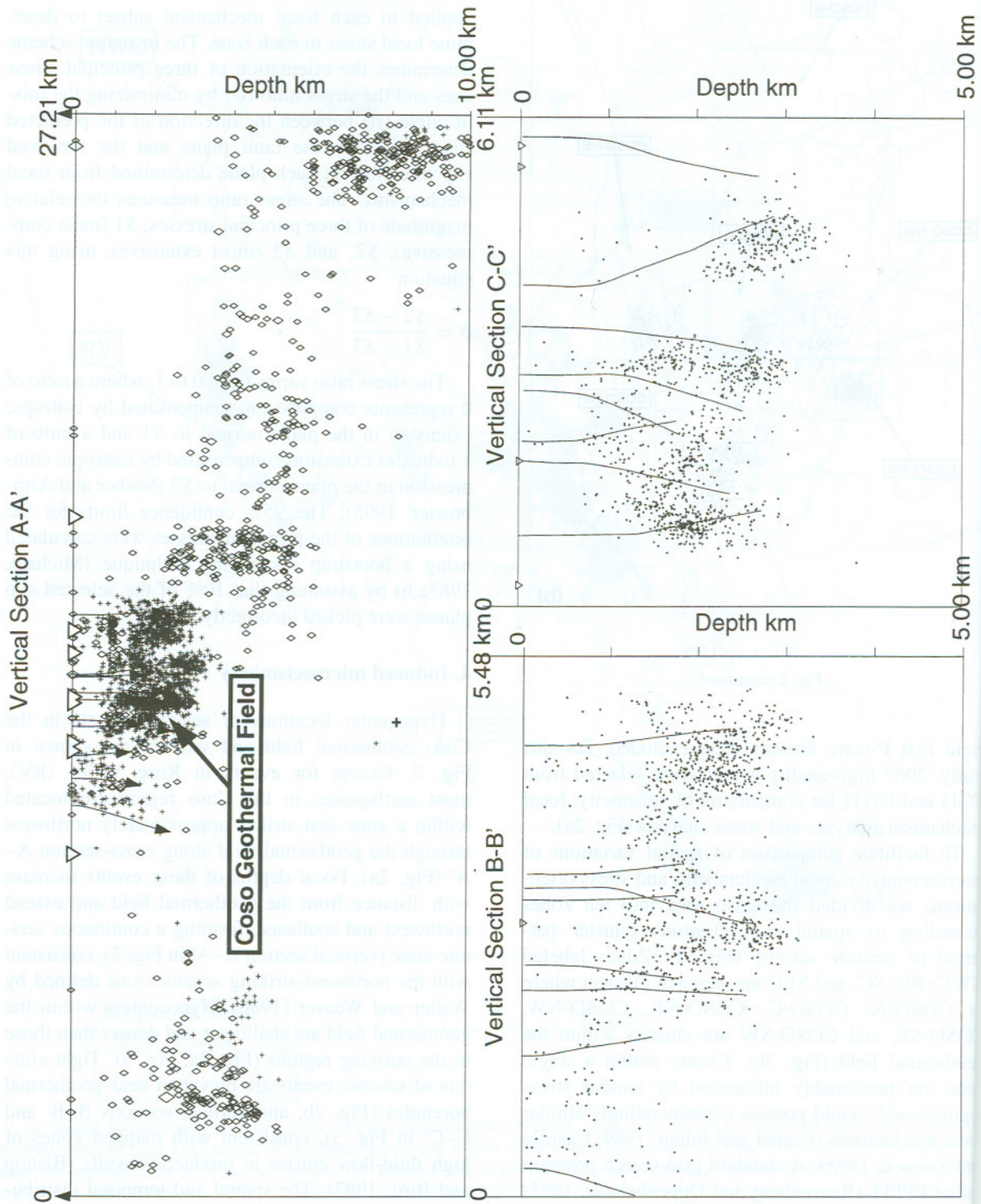
Depth km

27.21 km

10.00 km

0

Vertical Section A-A'

Coso Geothermal Field

Depth km

6.11 km

0

Vertical Section C-C'

5.00 km

Depth km

5.48 km

0

Vertical Section B-B'

5.00 km

Fig. 1. G
(closed li
principal

the pred
understa
the geot

that events in the geothermal field are associated with fluid injection and circulation (J. Copp, California Energy Co., pers. commun., 1994).

In the spring of 1992 a relatively large event was recorded west of the geothermal field near the Sierran front in Rose Valley (RV). Nearly all events in RV were recorded during the intense period of activity following the 1992 RV mainshock. This seismic sequence occurred along a north–south-trending fault and was not associated with geothermal activity (Roquemore and Simila, 1994).

The CITD and CGD data sets can be compared using histograms to clarify the temporal distribution between local microseismicity in the geothermal field and long-term regional seismicity (Fig. 4). Virtually no correlation between the two data sets for the same time period (Fig. 4b) is observed (correlation coefficient = 0.2). The large increase of events in CGD since September 1992 may be a result of the improved recording in the Coso Digital Seismic Network. The high seismic rates in CITD were primarily due to mainshock–aftershock sequences of the Mammoth Lakes ($M$ 6.2, 11/23/84) and Rose Valley events ($M$ 4, 2/19/92) (Roquemore and Simila, 1994). The CGD set has a higher microseismic rate than CITD after the improvement of recording capability of the Coso Digital Seismic Network. There was no apparent increase of seismicity in either data set immediately following the 1992 Landers earthquake sequence.

A recent, moderate-sized event ($M$ 5.0) was recorded in the Coso Geothermal region east-northeast of the producing field on 11/27/96 (Jim Mori, USGS, SCEC commun., 1994). Based on preliminary analysis, the event appears to have northeast and northwest nodal planes with aftershocks located along northeast–southwest orientation. Numerous aftershocks have been recorded on the microearthquake network, but these have not been catalogued or interpreted at the time of this writing.

## 5. Focal mechanism and stress

We obtained 2967 single-event, upper-hemisphere focal-plane solutions for earthquakes located in the Coso geothermal area and its vicinity. Average uncertainties of strike, dip, and rake, are 13°, 14°, 18°, respectively, for focal mechanisms in CGD, and 13°,

25°, 29°, respectively, for those in CITD. For each zone, focal mechanism P-axes were projected to a focal sphere, within which concentrations of P-axes are represented by graduated gray shades (Fig. 5). Stresses calculated from focal-plane solutions in the ten zones are summarized in Table 2 in terms of their eigenvalues, eigenvectors, and stress ratios ($\phi$). The orientations of the principal stresses and associated confidence limits with the stress axes are illustrated in Fig. 5.

The orientation of focal mechanisms and stress ellipses indicates approximate north–south compression and east–west extension along the northwest-trending seismic zone, consistent with previously inferred stress patterns in the Coso region (Walter and Weaver, 1980; Bacon et al., 1980; Roquemore, 1980, 1984). Within this setting, significant variations in focal mechanism and stress may be attributed to localized orientations of active faults and fracture zones. At the center of the geothermal field, including COSO-NE, COSO-C, COSO-NW, and COSO-SW (Fig. 5a), concentrations of P-axes and the maximum compressive stresses ($S1$) are consistent and tend to be vertical, except at COSO-SW, which exhibits a maximum compressive stress ($S1$) in the horizontal direction. North and southeast of the principal geothermal area, including COSO-N, COSO-SE, SC, and SEC (Fig. 5b), the maximum compressive stresses are primarily horizontal, in contrast to COSO-NE, COSO-C, and COSO-NW, and oriented north-northeast with varying strikes (Fig. 5b). Note the dispersion of P-axes concentrations as a result of the scattering of events over a large area. For all the eight zones, the stress ratios range from 0.69 to 0.86, indicating that the magnitude difference between $S1$ and $S2$ has decreased in the principal geothermal field.

The RV aftershocks have a sharp peak in concentration of P-axes and stress patterns (Fig. 5c), which can be attributed to the similarity of the focal mechanisms of the aftershocks to the focal mechanism of the 1992 ($M = 4$) Rose Valley event. The mapped fault for this sequence strikes approximately north–south, consistent with the calculated stress pattern in Fig. 5c. The stress ratio of RV is 0.53, which also indicates a well constrained strike-slip faulting. NWC, located northwest of the geothermal field, has a horizontal $S1$ trending nearly north–south
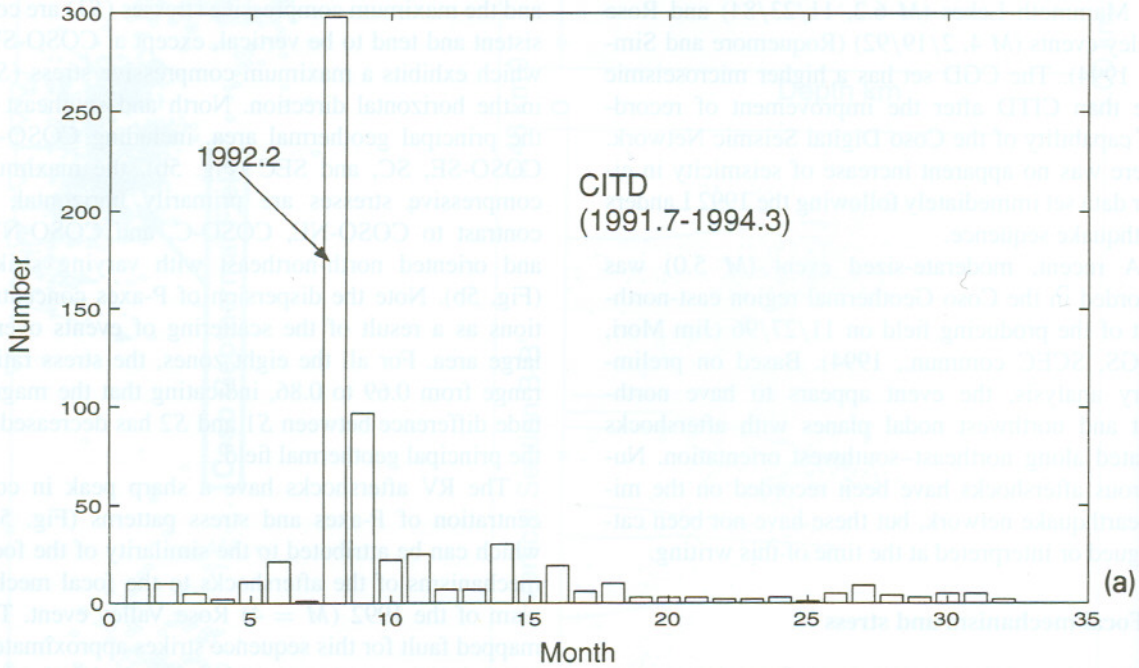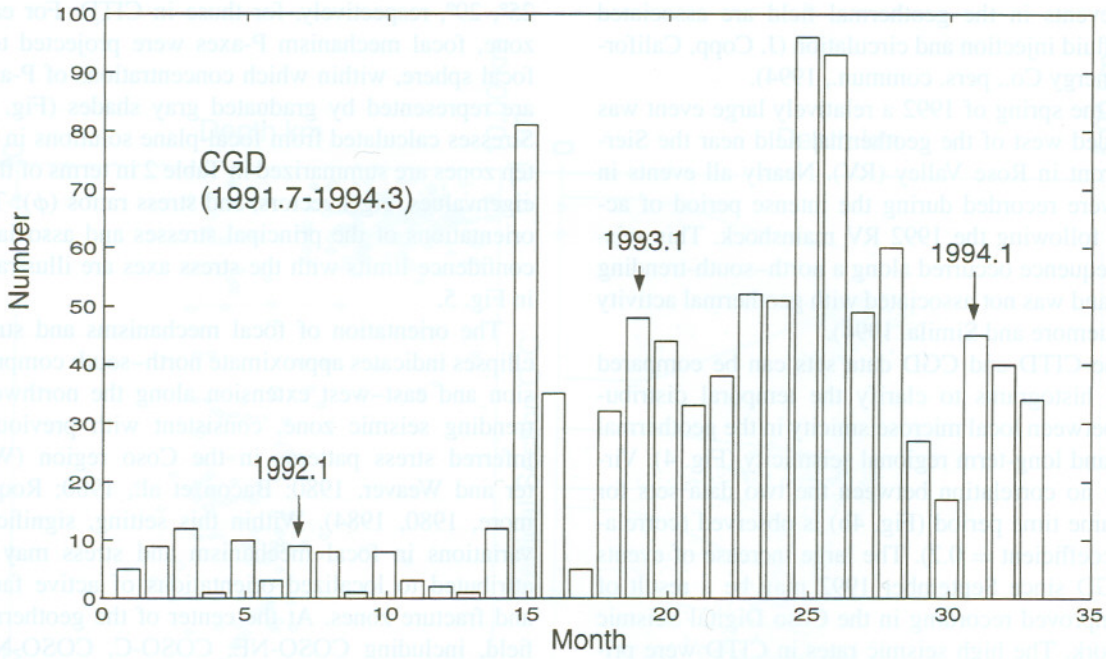
Fig. 4. Temporal histograms of all events from CGD (top) and CITD (bottom). All events from each data set are presented in (a) a those covering the same time period are presented in (b).
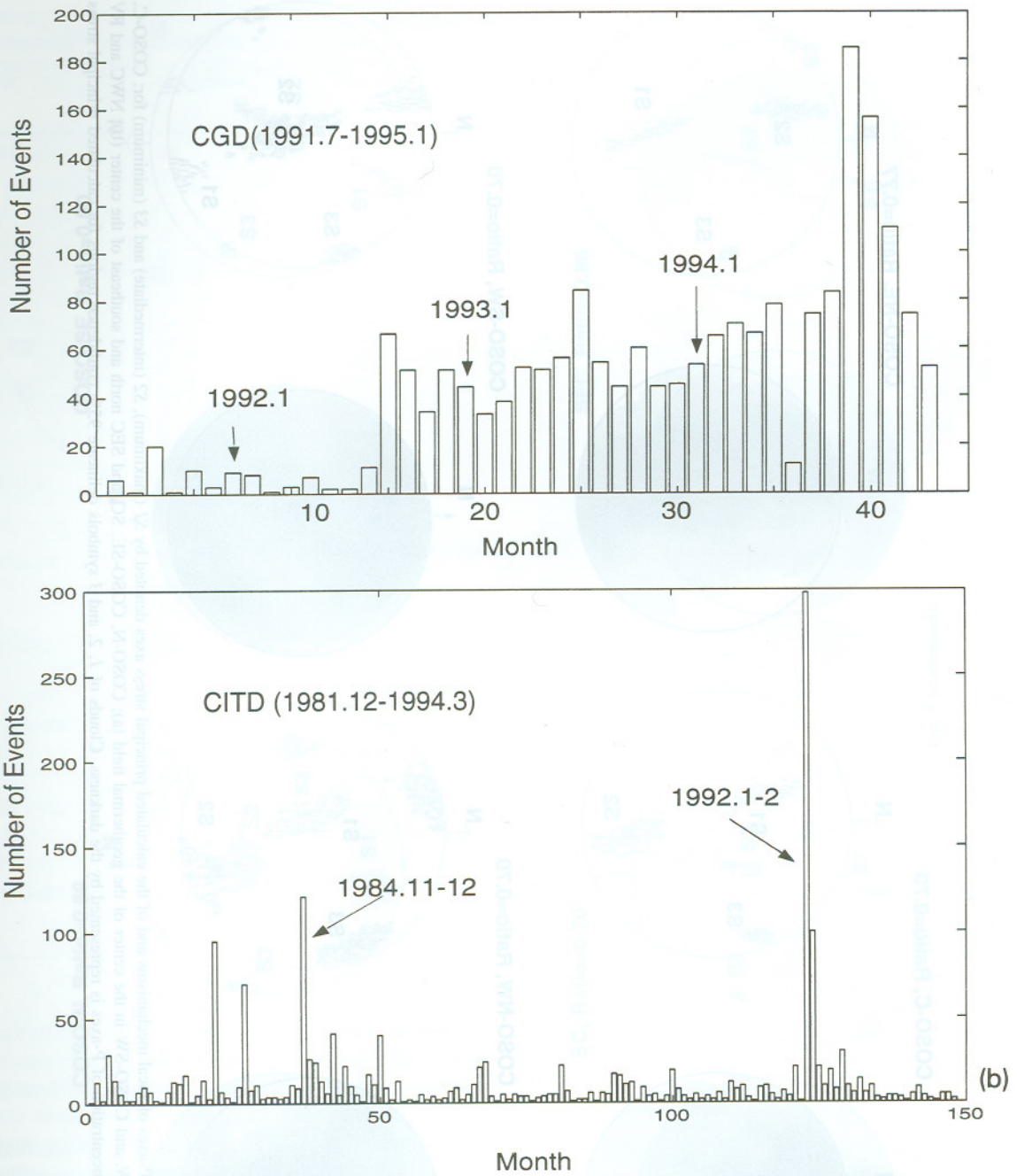
Fig. 4 (continued).

(Fig. 5c). Stress ratio for this zone is 0.4, similar to that of RV, suggesting the continuity of the compression stress west and northwest of the principal geothermal field.

## 6. Fracture zones and seismicity

Several studies outside the Coso area have observed a relationship between microseismic activity

COSO-C, Ratio=0.70

COSO-NE, Ratio=0.77

COSO-NW, Ratio=0.70
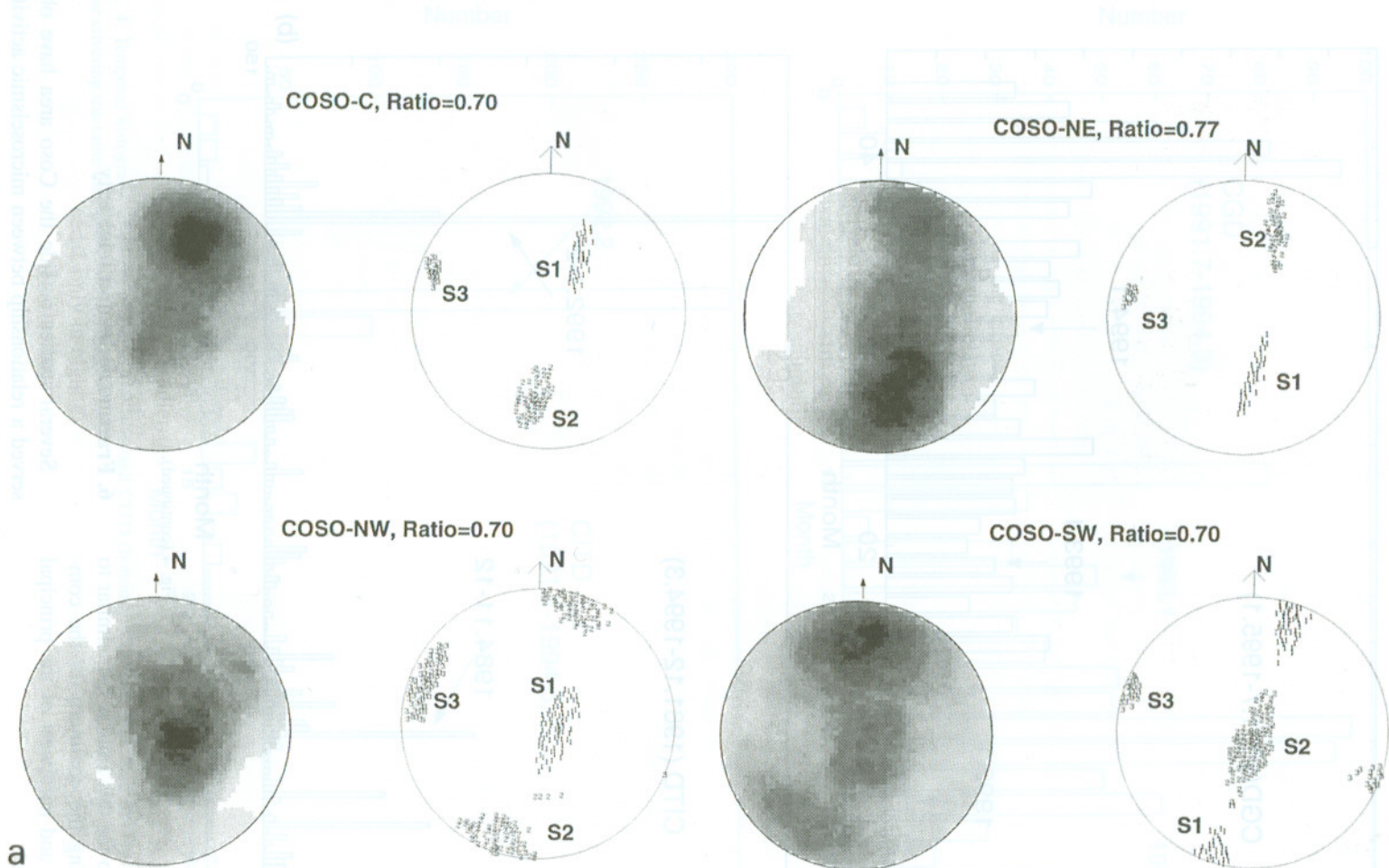
COSO-SW, Ratio=0.70

a

Fig. 5. Projections of P-axes of focal mechanisms and of the calculated principal stress axes denoted by *S1* (maximum), *S2* (intermediate) and *S3* (minimum) for: COSO-C, COSO-NE, COSO-NW, and COSO-SW in the center of the geothermal field (a); COSO-N, COSO-SE, SC, and SEC north and southeast of the center (b); NWC and RV in the vicinity (c). Concentration of P-axes is represented by the darkness. Clouds of *1*, *2*, and *3* symbols delineate 95% confidence regions for calculated principal stress directions.
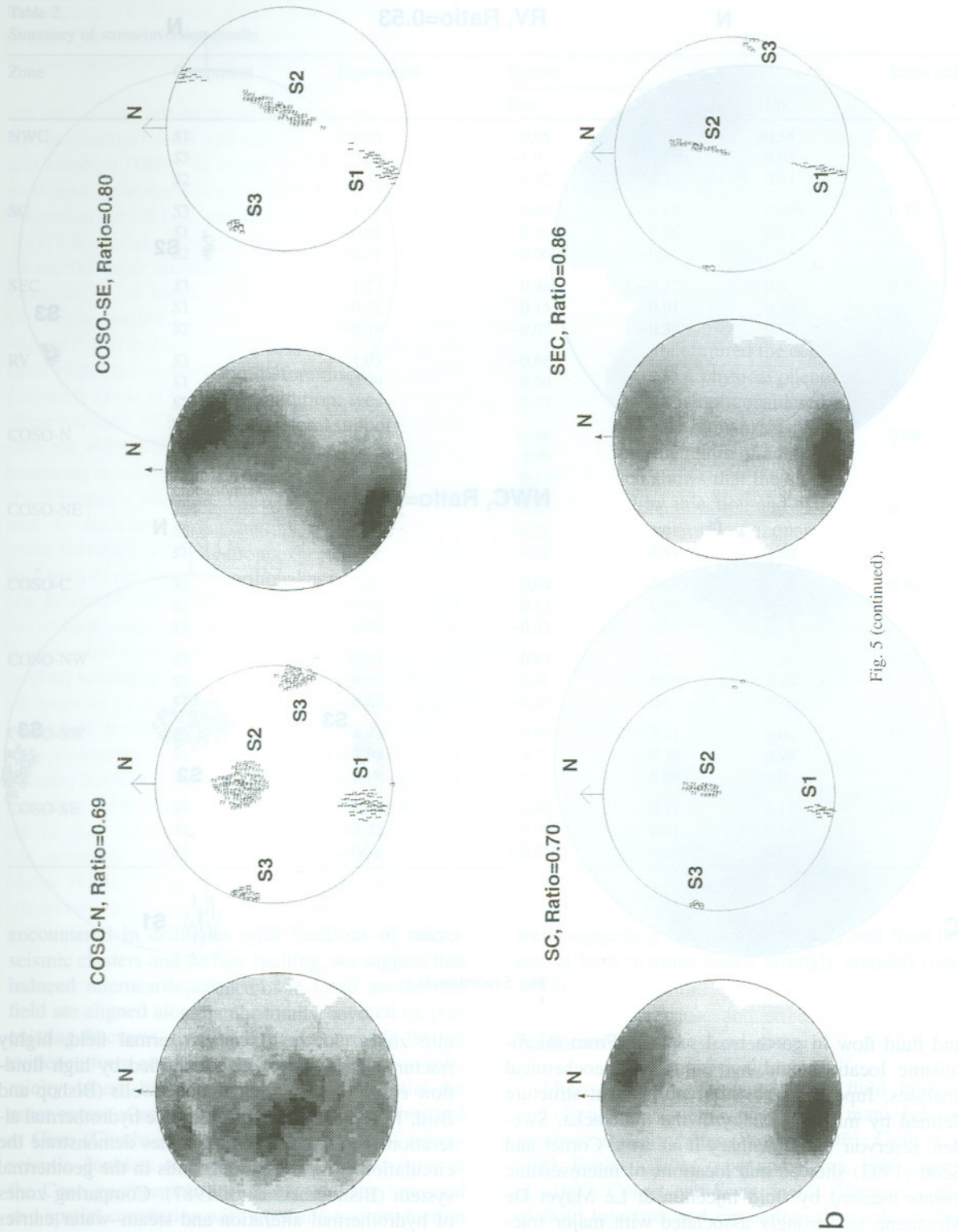
Fig. 5 (continued).
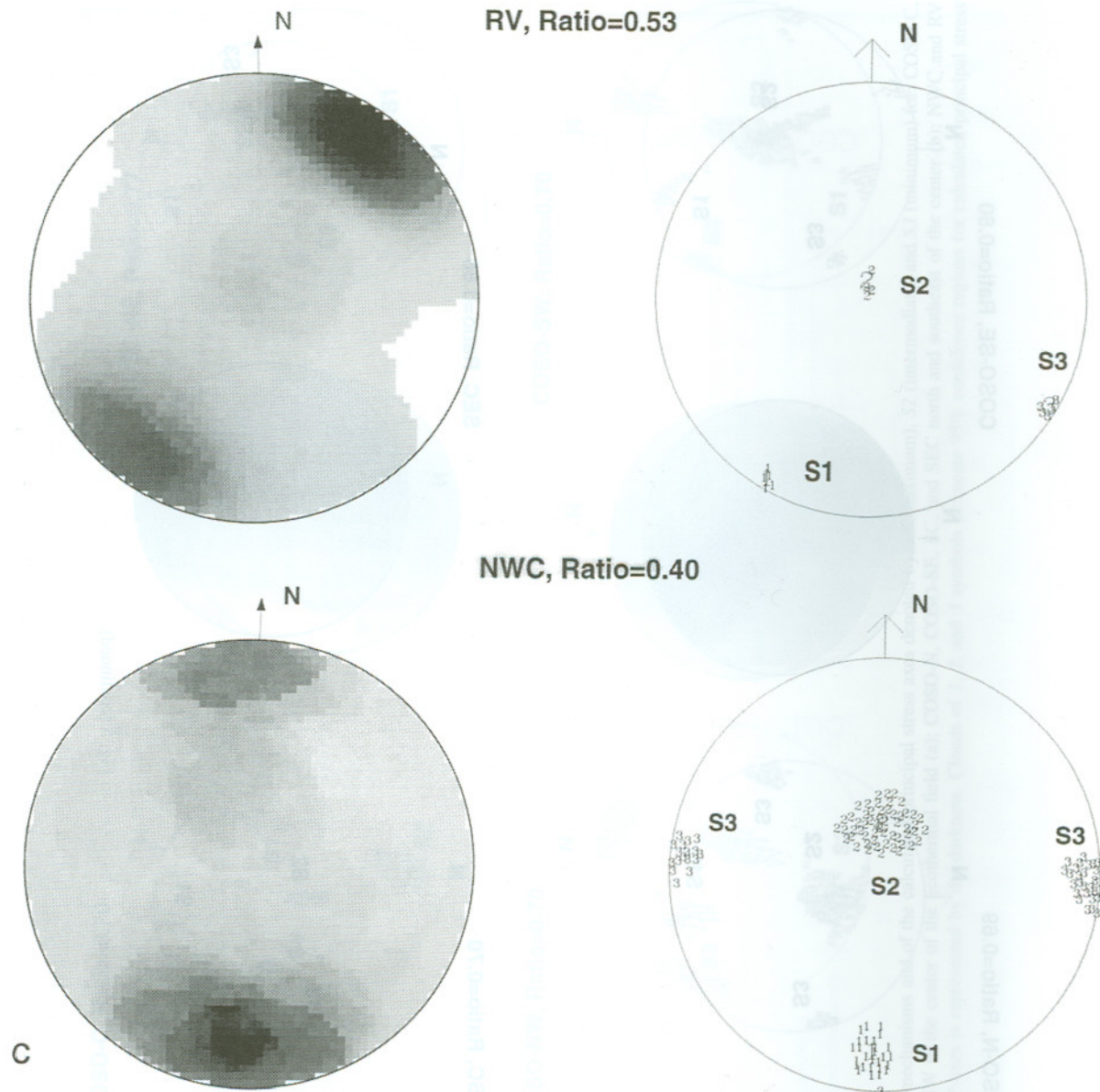
**RV, Ratio=0.53**

**NWC, Ratio=0.40**

Fig. 5 (continued).

and fluid flow in geothermal settings. From microseismic locations and hydraulic and geochemical analyses, Jupe et al. (1992) reported that structure defined by microseismicity in the Fjällbacka, Sweden, reservoir is the primary fluid path. Cornet and Scott (1993) showed that locations of microseismic events induced by fluid injection at Le Mayet De Montagne are strongly associated with major fracture zones. In the Coso geothermal field, highly fractured zones have been identified by high fluid-flow entry zones in development wells (Bishop and Bird, 1987). Surface and subsurface hydrothermal alterations near these fractured zones demonstrate the circulation of hydrothermal fluids in the geothermal system (Bishop and Bird, 1987). Comparing zones of hydrothermal alteration and steam–water entries

Table 2
Summary of stress-inversion results

| Zone | Component | Eigenvalues | Vectors | | | Stress ratio |
| --- | --- | --- | --- | --- | --- | --- |
| | | | East | North | Up | |
| NWC | S1 | -1.06 | 0.05 | 0.94 | 0.34 | 0.40 |
| | S3 | 0.94 | -1.0 | 0.04 | 0.03 | |
| | S2 | 0.12 | 0.12 | -0.34 | 0.93 | |
| SC | S3 | 1.15 | 0.99 | -0.17 | 0.026 | 0.70 |
| | S1 | -0.88 | 0.16 | 0.96 | 0.21 | |
| | S2 | -0.27 | -0.06 | -0.20 | 0.98 | |
| SEC | S3 | 1.27 | 0.98 | -0.17 | 0.0 | 0.86 |
| | S1 | -0.78 | 0.15 | 0.91 | 0.39 | |
| | S2 | -0.49 | -0.07 | -0.38 | 0.92 | |
| RV | S3 | 1.03 | -0.86 | 0.50 | 0.08 | 0.53 |
| | S1 | -0.99 | 0.50 | 0.86 | 0.09 | |
| | S2 | -0.04 | 0.03 | -0.12 | 0.99 | |
| COSO-N | S3 | 1.01 | -0.98 | 0.0 | 0.17 | 0.69 |
| | S1 | -0.79 | 0.09 | 0.87 | 0.48 | |
| | S2 | -0.22 | 0.15 | -0.48 | 0.86 | |
| COSO-NE | S3 | 1.27 | 0.95 | -0.17 | 0.26 | 0.77 |
| | S3 | -0.39 | -0.28 | -0.81 | 0.52 | |
| | S1 | -0.88 | -0.12 | 0.57 | 0.82 | |
| COSO-C | S3 | 1.0 | 0.94 | -0.29 | 0.18 | 0.70 |
| | S2 | -0.23 | 0.13 | 0.79 | 0.60 | |
| | S1 | -0.78 | -0.31 | -0.54 | 0.78 | |
| COSO-NW | S3 | 0.82 | 0.91 | -0.35 | 0.21 | 0.7 |
| | S2 | -0.19 | 0.31 | 0.93 | 0.18 | |
| | S1 | -0.62 | -0.26 | -0.1 | 0.96 | |
| COSO-SW | S3 | 0.77 | 0.95 | -0.31 | 0.02 | 0.7 |
| | S1 | -0.59 | -0.31 | -0.95 | 0.08 | |
| | S2 | -0.18 | 0.0 | 0.08 | 1.0 | |
| COSO-SE | S3 | 1.09 | 0.89 | -0.42 | 0.17 | 0.8 |
| | S1 | -0.72 | 0.39 | 0.91 | 0.16 | |
| | S2 | -0.36 | -0.21 | -0.08 | 0.97 | |

encountered in drillholes with locations of microseismic clusters and surface faulting, we suggest that induced microearthquakes in the Coso geothermal field are aligned along, and can be attributed to, pre-existing fractures. Heat-flow studies provide further evidence for a correlation of fracture and microseismicity, where high heat-flow contours parallel the outer extent of active microseismic clusters observed at Coso (Combs, 1980). Finally, analysis of microseismic doublets and multiplets (similar events) in the Coso geothermal field shows a strong temporal and spatial correlation with injection and production

wells suggesting that microseismicity and fluid flow are, at least in some cases, strongly coupled (Lees, 1995).

## 7. Discussion

Microseismicity associated with fluid injection and circulation has been observed in many hot-rock geothermal energy sites (Pearson, 1981; Cash et al., 1983; Fehler, 1989; Cornet and Julien, 1989; Jupe et al., 1992; Cornet and Scott, 1993). The mechanism of fluid injection and circulation that induces frac-

tures can be explained by theories of effective stress and Coulomb–Mohr shear failure (Scholz, 1990). Fluid injection increases pore pressure and reduces effective stress, resulting in hydrofracturing and inducing microseismicity. For the case at Coso, where the vast majority of the wells produce from flows through pre-existing fractures (F. Monastero, Navy Geothermal Program Office, pers. commun., 1994), fluid injection and circulation probably results in local stress perturbations and activation of shearing along the major pre-existing fractures.

Calculated stresses from focal mechanisms help to detail the variations of localized stresses and identify a transition from a transtensional regime in the principal geothermal area to a transpressional regime southeast and northwest of the geothermal center (Figs. 6 and 7). The stress transition in the geothermal field generally coincides with the spatial distribution of major faults as illustrated by the correlation of $S1$ with mapped faults. COSO-NE, COSO-C, and COSO-NW each have large, vertical $S1$ components (Figs. 6 and 7) that lie along normal fault zones trending north-northeast. COSO-N, COSO-SE, SC, and SEC have large horizontal $S1$ components aligned along mapped northwest-striking faults (Fig. 7). The correlation of mapped faults with calculated stress distributions suggests that orientations of the pre-existing fractures are consistent with the surface-mapped faults. COSO-SW, how-

ever, shows a very small vertical $S1$ component (Fig. 6), though it is located immediately adjacent to COSO-NW and normal fault zones which apparently trend north-northeast.

A similar stress variation to the above was observed at Fenton Hill Hot Dry Rock Geothermal Site (Cash et al., 1983). Cash et al. (1983) reported that $S1$ changed considerably from horizontal orientation in the deeper reservoir (about 1–1.5 km) to vertical orientation in the upper reservoir (about 0.5 km). They suggested that the transition from horizontal to vertical orientation was caused by a subsiding magma chamber under Valles Caldera, where the lower reservoir is closer to the Caldera rim. The subsiding magma chamber can cause anomalously large horizontal stresses due to arching in rocks overlying the chamber (Cash et al., 1983). This does not apply at Coso, where COSO-NW and COSO-SW are both located close to the magma source that is presumed to be several kilometers beneath this region. Effects of topography, overburden, and variation of heat gradients within the geothermal field provide alternative mechanisms for the observed stress transition between COSO-NW and COSO-SW. Meertens and Wahr (1986) showed that surface slopes tend to rotate maximum compressive stress away from vertical towards the orientation of the sloping ground surface, and a thick surface overburden tends to increase the normal stress component. For the effects of thermal stress, Batzle (1978) pointed out that increasing temperature can cause fluid pressure in isolated pores to increase a sufficient amount to cause either widening of pre-existing fractures or failure of rock in the direction of greatest principal stress. However, the close proximity of COSO-NW to COSO-SW would appear to preclude these physical mechanisms for the apparent source of variation within each respective stress field.

COSO-SW and COSO-NW are in close spatial proximity although they differ significantly in their respective stress orientation. The difference may be attributed to structural variations where each cluster occurs in a geologically isolated block. Variations in seismic-wave attenuation observed in this region (Wu and Lees, 1996), where COSO-NW has low $Q$ quality factor (high attenuation) compared to high $Q$ seen in COSO-SW seem to support the observation that these are structurally separate zones. High heat-
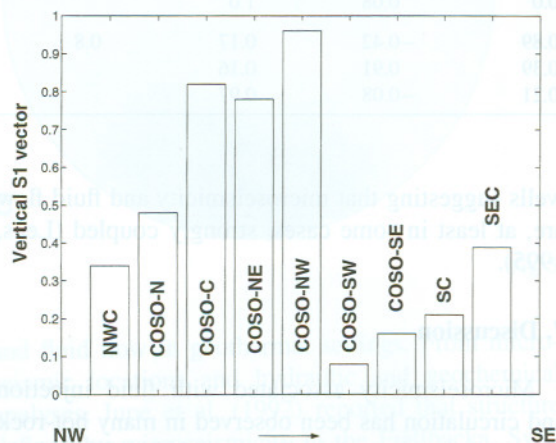


Fig. 6. Spatial variation of vertical $S1$ eigenvectors northwest to southeast along the northwest-trending seismic zone. Note that the COSO-SW cluster has the smallest $S1$ component, significantly different from adjacent COSO-NW.
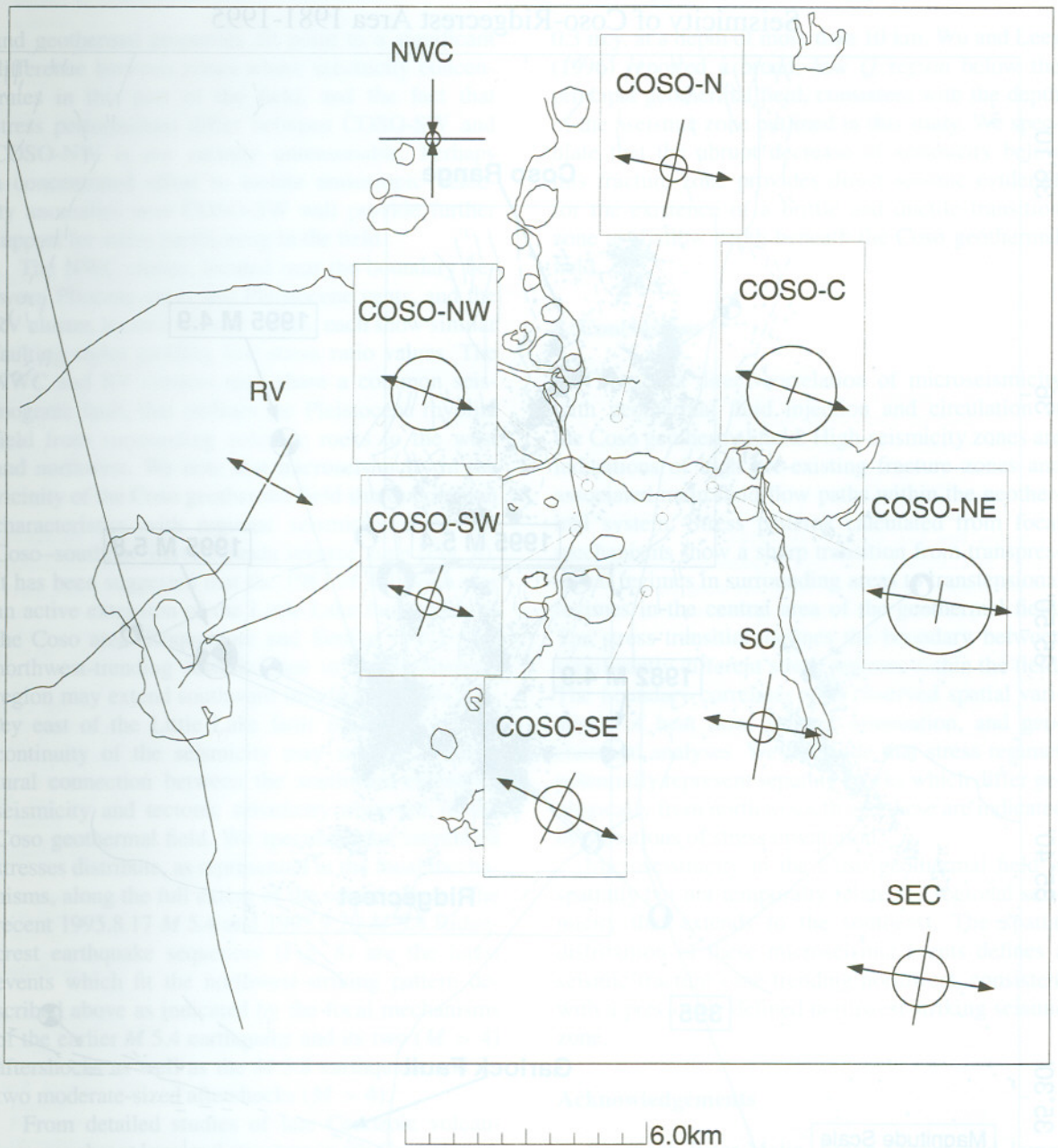
Fig. 7. Map view of variation of principal stress axes in each zone. Principal stress axes are plotted as segments for nearly horizontal components and as circles for nearly vertical components. Lengths of segments and radii are proportional to eigenvalues of corresponding components. Arrows indicate polarity of the largest components, inward for negative and outward for positive.

flow gradients between the two clusters (Combs, 1980) further supports the separation of these clusters into two separate stress regimes. The geochemical analyses of production fluids and fluid inclusions indicate that the COSO-SW cluster is located in a region of concentrated Cl and $CO_2$, which drop off significantly in the COSO-NW zone (Moore et al., 1989). The variations of geophysical, geochemical

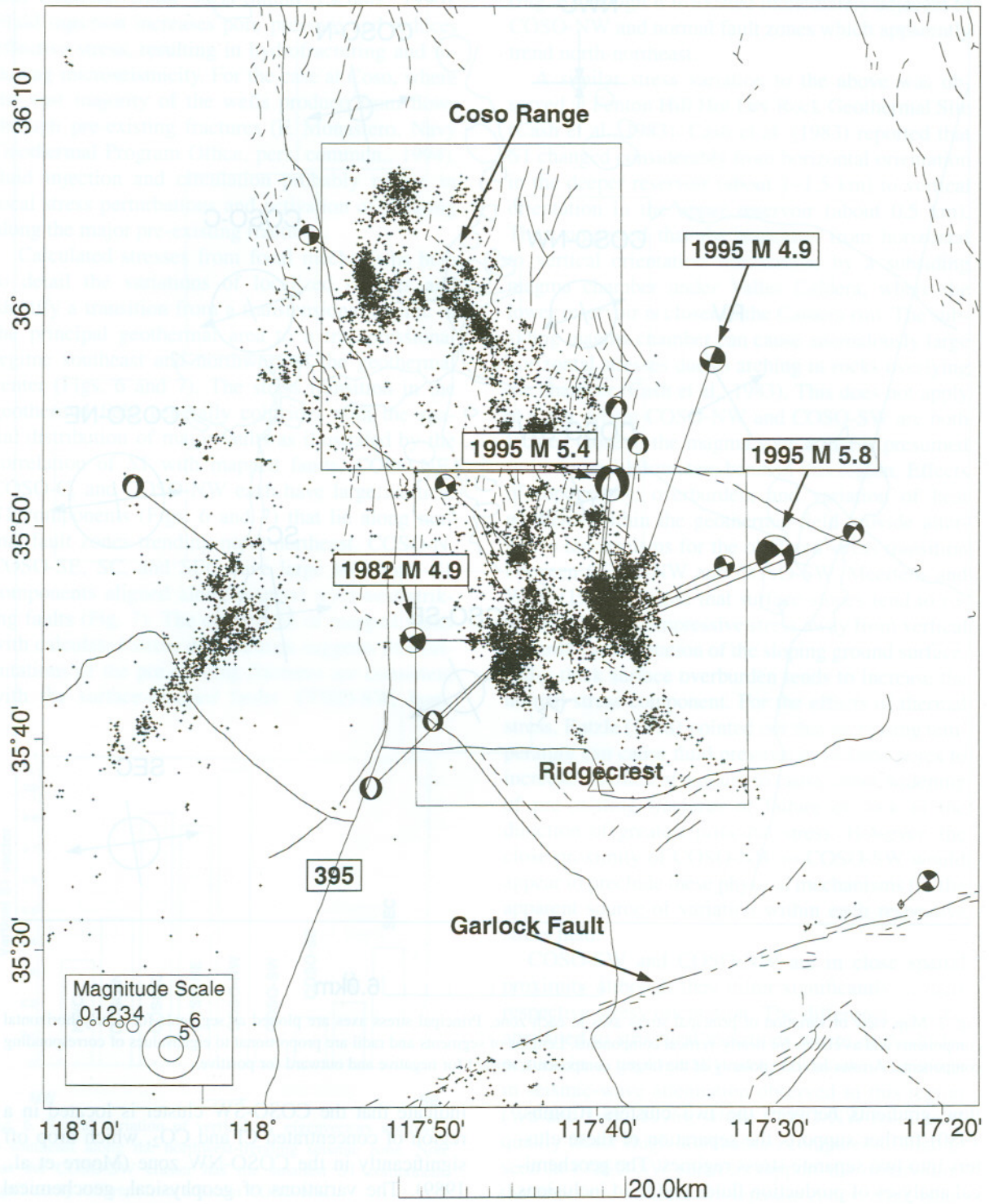## Seismicity of Coso-Ridgecrest Area 1981-1995



Fig. 1
(close
princi

the p
unde
the g

and geothermal properties all point to a significant difference between zones where seismicity concentrates in this part of the field, and the fact that stress perturbations differ between COSO-SW and COSO-NW is not entirely unreasonable. Perhaps a concentrated effort to isolate anisotropic velocity anomalies near COSO-SW will provide further support for stress partitioning in the field.

The NWC cluster, located near the boundary between Pliocene vents and Pleistocene vents, and the RV cluster, located in Rose Valley, each show similar faulting styles yielding low stress ratio values. The NWC and RV clusters may share a common seismogenic fault, that outlines the Pleistocene rhyolite field from surrounding volcanic rocks to the west and northwest. We note that microseismicity in the vicinity of the Coso geothermal field shares common characteristics with regional seismicity along the Coso–southern Sierra Nevada seismic zone (Fig. 8). It has been suggested that the 1982 *M* 4.9 event was an active extension of the Little Lake fault south of the Coso area (Roquemore and Simila, 1994). The northwest-trending seismic zone in the geothermal region may extend southward into Indian Wells Valley east of the Little Lake fault zone. The spatial continuity of the seismicity may suggest a structural connection between the southward-extending seismicity and tectonic seismicity observed in the Coso geothermal field. We speculate that correlated stresses distribute, as represented in the focal mechanisms, along the full extent of the seismic zone. The recent 1995.8.17 *M* 5.4 and 1995.9.20 *M* 5.8 Ridgecrest earthquake sequences (Fig. 8) are the latest events which fit the northwest-striking pattern described above as indicated by the focal mechanisms of the earlier *M* 5.4 earthquake and its two (*M* > 4) aftershocks as well as the *M* 5.8 earthquake and its two moderate-sized aftershocks (*M* > 4).

From detailed studies of late Cenozoic volcanism, geochronology and structure in the Coso Range, Duffield et al. (1980) suggest that the Coso geothermal system is sustained by heat from a crustal silicic magma reservoir that has existed for at least the last

0.3 m.y. at a depth of more than 10 km. Wu and Lees (1996) reported a broad, low *Q* region below the principal geothermal field, consistent with the depth of the aseismic zone outlined in this study. We speculate that the abrupt decrease of seismicity below this fracture zone provides direct seismic evidence for the existence of a brittle and ductile transition zone at shallow depth beneath the Coso geothermal field.

## 8. Conclusions

There is a direct correlation of microseismicity with geothermal fluid injection and circulation at the Coso geothermal field. High-seismicity zones are indications of high pre-existing fracture zones and associated main fluid-flow paths within the geothermal system. Stress patterns calculated from focal mechanisms show a sharp transition from transpressional regimes in surrounding areas to transtensional regimes in the central area of the geothermal field. The stress transition defines the boundary between significantly different stress regimes within the field. The boundary correlates with observed spatial variations of heat flow, seismic attenuation, and geochemical analyses. We conclude that stress regimes potentially represent separate blocks which differ geologically from north to south and these are indicated by variations of stress orientation.

Microseismicity in the Coso geothermal field is spatially but not temporally related to regional seismicity that extends to the southeast. The spatial distribution of these microseismic events defines a seismic-fracture zone trending northwest, consistent with a previously defined northwest-striking seismic zone.

## Acknowledgements

17°20'

Fig. 8. Regional seismicity in the Coso–southern Sierra Nevada area from 1981 to 1995, including the 1995 *M* 5.4 and *M* 5.8 Ridgecrest sequences and 1982 *M* 4.9 Ridgecrest sequence. Boxes outline the Coso Range (Figs. 1 and 2) and the Ridgecrest area. Focal mechanisms are given for larger events (*M* > 4).

provided critical reviews that helped to improve the manuscript. The authors acknowledge the Navy Geothermal Program for funding this project (award N68936-94-R-0139) and providing data.

# References

Bacon, C.R., Duffield, W.A., Nakamura, K., 1980. Distribution of Quaternary rhyolite domes of the Coso Range, California: implications for extent of the geothermal anomaly. J. Geophys. Res. 85 (B5), 2422–2433.

Batzle, M.L., 1978. Fracturing and Sealing in Geothermal Systems. Ph.D thesis, MIT, Cambridge, MA.

Bishop, B.P., Bird, D.K., 1987. Variation in sericite compositions from fracture zones within the Coso Hot Springs geothermal system. Geochim. Cosmochim. Acta 51, 1245–1256.

Cash, D., Homuth, E.F., Keppler, H., Pearson, C., Sasaki, S., 1983. Fault plane solutions for microearthquakes induced at the Fenton Hill Hot Dry Rock Geothermal Site: implications for the state of stress near a Quaternary volcanic center. Geophys. Res. Lett. 10 (12), 1141–1144.

Castillo, D.A., Zoback, M.D., 1995. Systematic stress variations in the southern San Joaquin Valley and along the White Wolf fault: Implications for the rupture mechanics of the 1952 $M_s$ 7.8 Kern County earthquake and contemporary seismicity. J. Geophys. Res. 100 (B4), 6249–6264.

Combs, J., 1980. Heat flow in the Coso geothermal area, Inyo County, California. J. Geophys. Res. 85 (B5), 2411–2424.

Cornet, F.H., Julien, P., 1989. Stress determination from hydraulic test data and from mechanisms of induced seismicity. Int. J. Rock Mech. Min. Sci. Geomech. Abstr. 26 (3/4), 235–248.

Cornet, F.H., Scott, O., 1993. Analysis of induced seismicity for fault zone identification . Int. J. Rock Mech. Min. Sci. Geomech. Abstr. 30 (7), 789–795.

Duffield, W.A., Bacon, C.R., Dalrymple, G.B., 1980. Late Cenozoic volcanism, geochronology, and structure of the Coso Range, Inyo County, California. J. Geophys. Res. 85 (B5), 2381–2404.

Fehler, M.C., 1989. Stress control of seismicity patterns observed during hydraulic fracturing experiments at the Fenton Hill Hot Dry Rock Geothermal Energy Site, New Mexico. Int. J. Rock Mech. Min. Sci. Geomech. Abstr. 26 (3/4), 211–219.

Jupe, A.J., Green, A.S.P., Wallroth, T., 1992. Induced microseismicity and reservoir growth at the Fjällbacka hot dry rocks project, Sweden. Int. J. Rock Mech. Min. Sci. Geomech. Abstr. 29 (4), 343–354.

Lees, J.M., 1995. Seismic doublets in the Coso Geothermal Field. EOS Trans. AGU 76 (46), Fall Meeting Suppl., F407.

Meertens, C.M., Wahr, J.M., 1986. Topographic effects on tilt, strain, and displacement measurements. J. Geophys. Res. 91, 14057–14062.

Michael, A.J., 1984. Determination of stress from slip data: faults and folds. J. Geophys. Res. 89, 11517–11526.

Michael, A.J., 1987a. The use of focal mechanisms to determine stress: a control study. J. Geophys. Res. 92, 357–368.

Michael, A.J., 1987b. Stress rotation during the Coalinga aftershock sequence. J. Geophys. Res. 92, 7963–7979.

Moore, J.N., Adams, M.C., Bishop, B.P., Hirtz, P., 1989. A fluid flow model of the Coso geothermal system: data from production fluids and fluid inclusions. Proc., 14th Workshop Geothermal Reservoir Engineering, January 24–26, Stanford University, Stanford, CA, pp. 139–144.

Pearson, C., 1981. The relationship between microseismicity and high pore pressures during hydraulic stimulation experiments in low permeability granitic rocks. J. Geophys. Res. 86 (B9), 7855–7864.

Reasenberg, P., Oppenheimer, D., 1985. FPFIT, FPPLOT and FPPAGE: Fortran computer programs for calculating and displaying earthquake fault-plane solutions. U.S. Geol. Surv. Open-File Rep. 85-739, 109 pp.

Roquemore, G.R., 1980. Structure, tectonics, and stress field of the Coso Range, Inyo County, California. J. Geophys. Res. 85 (B5), 2434–2440.

Roquemore, G.R., 1984. Ground magnetic survey in the Coso Range, California. J. Geophys. Res. 89 (B5), 3309–3314.

Roquemore, G.R., Simila, G.W., 1994. Aftershocks from the 28 June 1992 Landers earthquake: northern Mojave Desert to the Coso volcanic field, California. Bull. Seismol. Soc. Am. 84 (3), 854–862.

Scholz, C.H., 1990. The Mechanics of Earthquakes and Faulting. Cambridge University Press, New York.

Seeber, L., Armbruster, J.G., 1995. The San Andreas fault system through the Transverse Ranges as illuminated by earthquakes. J. Geophys. Res. 100 (B5), 8285–8310.

Walter, A.W., Weaver, C., 1980. Seismicity of the Coso Range, California. J. Geophys. Res. 85 (B5), 2441–2458.

Wohletz, K., Heiken, G., 1992. Volcanology and Geothermal Energy. University of California Press, Berkeley, CA.

Wu, H., Lees, J., 1996. Attenuation structure of Coso geothermal area, California, from wave pulse widths. Bull. Seismol. Soc. Am. 86 (5), 1574–1590.